Ain Shams University,Engineering Bulletim

Vol. 25, No. 3, Dec., 1990, Page. 106-131

MATHEMATICAL MODEL FOR PREDICTING THE PROPERTIES OF THE HYDRAULIC JUMP OVER ROUGH BEDS

Sharl S. Sakla[1], *Mohamed A. El-Samanoudy*[2], *Mahmoud H. El-Gamal*[3], *and Amro M. El-Feki*[4]

1 Prof. and Head of Irri. and Hydr. Dept., El-Mansoura Univ.
2 Assoc. Prof., Dept. of Irri. and Hydr., Ain Shams Univ.
3 Lecturer, Irri. and Hydr. Dept., El-Mansoura Univ.
4 Assist. Lecturer Irri. and Hydr. Dept., El-Mansoura Univ.

ABSTRACT

A mathematical model for predicting the properties of the hydraulic jump occurring over smooth and rough beds is presented. This mathematical model adopts the theoretical relations of the hydraulic jump over rough beds. The significant effect of bed roughness is included in the theoretical relations. Experimental results are quoted to check the validity of the proposed model. The results obtained for the various parameters of the hydraulic jump over the rough bed using the present mathematical model are compared with the respective experimental results. The trend of the experimental results is consistent with the theoretical prediction, and some good agreement between the results is achieved in the present study.

1. INTRODUCTION

The theoretical relations of the various parameters of the hydraulic jump derived in ref. [1] are used to form a mathematical model to predict the various parameters of the hydraulic jump over rough beds. The one-dimensional momentum equation of the hydraulic jump in this model includes the significantly important effect of the rough bed shear stress. Various mathematical expressions are obtained for the jump parameters such as the jump length, the conjugate depth, the total energy loss and the integrated bed shear force. The experimental work carried out by El-Feki [1] is then used to check the validity of the mathematical model. In these experiments free hydraulic jumps are formed downstream weir models of different geometrical scale ratios. The results obtained for the various parameters of the hydraulic jump over the rough bed using this mathematical model are compared with the respective experimental results.

2. THE MODEL NUMERICAL SCHEME

The definition diagram of Fig. 1 presents the principle variables and model of experimental operation used for creating the hydraulic jump over the rough bed. The apparatus supply tank provides the centrifugal pump with water to feed the entrance tank and the upstream channel.

Then the water flows over the weir model as shown in Fig. 1. The shooting (supercritical) flow created at the foot of the weir model converts into the tranquil (subcritical) flow by the formation of the hydraulic jump in the downstream of the weir model.

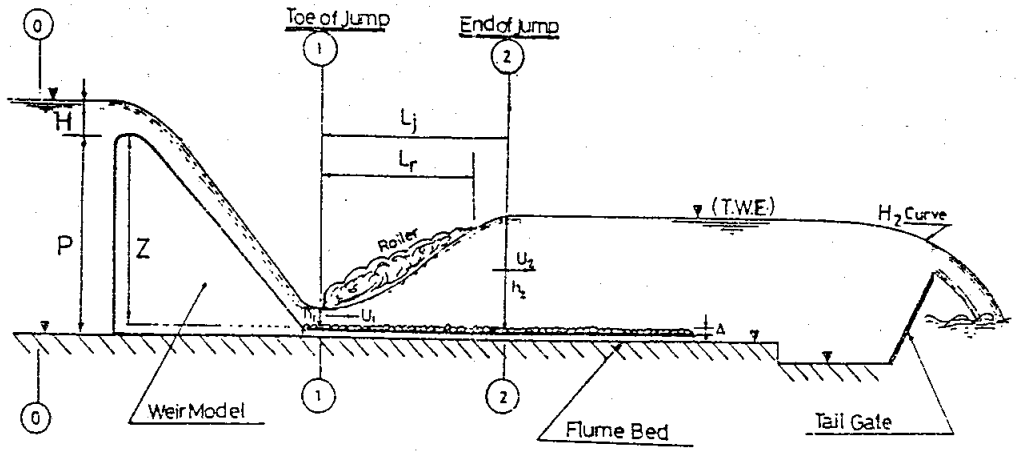

Fig. (1) Definition Sketch of The Flow Pattern Downstream Weir Model.

The flume tail gate is used to control the downstream depth of the hydraulic jump. The flume downstream depth is controlled to ensure that the jump formation would begin at the foot of the weir model.

The mathematical model is therefore applied to predict the properties of the hydraulic jump occurring over the rough test bed downstream the weir model. Both the values of the roughness height of the test bed and the flume rate of discharge are required to begin the calculation for predicting the various variables of the hydraulic jump. The flowchart of the numerical scheme is given in Fig. 2.

The weir model discharge equation is given by

$$Q = C_o H^{m_o} \qquad (1)$$

in which,

Q = Discharge of the weir model,

H = Head over the weir model, and

C_o, m_o = Constants for each weir model.

Ref. [1] gives the values of C_o and m_o obtained from various weir models.

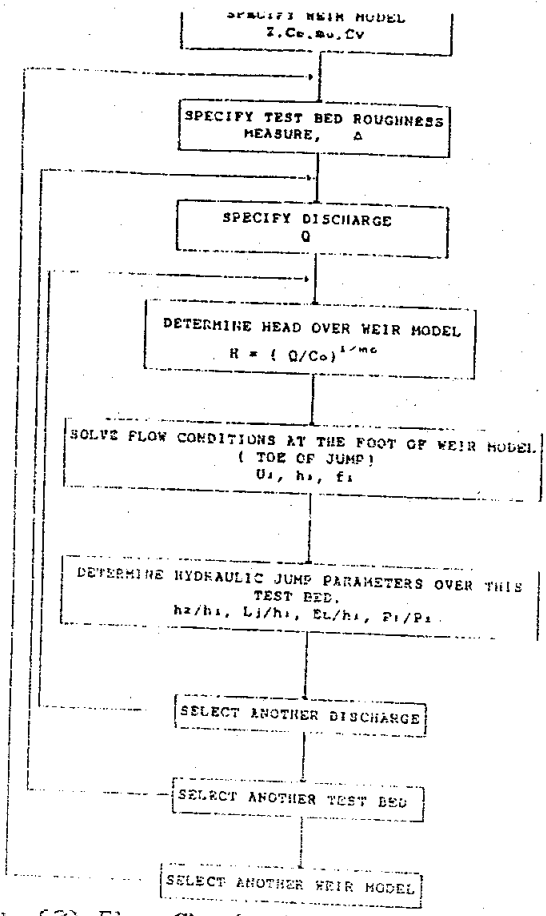

Fig. (2) Flow Chart of Numerical Scheme.

The solution of Eq. 1 for the head over the weir model is given by,

$$H = \sqrt[mo]{\left[\frac{Q}{Co}\right]} \qquad (2)$$

The depth or flow at the foot of each weir model can be calculated from application of the Bernoulli's equation for the flow between sections 0-0 and 1-1 as shown in Fig. 1,

$$Eo = E_1 + h_{L_{o\longrightarrow 1}} \qquad (3)$$

where

Eo = specific energy upstream of the weir model, at section 0-0,

E_1 = specific energy at section 1-1 (at the foot of the weir model), and

$h_{L_{o\longrightarrow 1}}$ = the energy loss across the weir model.

Also, the upstream specific energy may be given by

$$Eo = Zo + H \qquad (4)$$

in which

Zo = Effective drop height for each weir model, and

H = total head of water over the weir model includes the effect of the velocity head of the approaching flow.

The specific energy at the foot of the weir model E_1 may also be expressed by the following

$$E_1 = h_1 + \frac{U_1^2}{2g} \tag{5}$$

The substitution from Eq. 4 and Eq. 5 into Eq. 3 leads to the following equation

$$H + Z_o = h_1 + \frac{U_1^2}{2g} + h_{L_{o \longrightarrow 1}} \tag{6}$$

Eq. 6 may be simplified to give the following relation for the mean velocity of the flow at the foot of the weir model (inlet velocity of the hydraulic jump)

$$U_1 = C_v \sqrt{2g \left[H + Z_o - h_1 \right]} \tag{7}$$

where, C_v = coefficient of velocity which is mainly affected by the weir drop height Z_o

Since $$U_1 = Q / W h_1 \tag{8}$$

where, W = channel width.

The substitution for U_1 from Eq. 8 into Eq. 7 gives,

$$h_1 = \frac{Q}{C_v W \sqrt{2g \left[H + Z_o - h_1 \right]}} \tag{9}$$

The value of C_v for each weir model are given in ref. [1].

Eq. 9 is an implicit equation of the water depth h_1 at the foot of the weir model. Thus this equation may be solved using an iterative technique to obtain the supercritical flow depth h_1. For the supercritical flow of section 1-1 we have h_1 should be less than the critical depth h_{cr}.

Thus, $$h_1 < h_{cr}$$

where,

$$h_{cr} = \sqrt[3]{\frac{Q^2}{g W^2}} \tag{10}$$

The iterative scheme assumes an initial value for h_1 less than the value of h_{cr} and continues the calculations to get the value of h_1 in number of iteration until the difference in the value of the calculated h_1 between two successive iterations is less than 10^{-5} m (chosen for the accuracy in the calculation of h_1). Then, this value of h_1 is considered to be the appropriate solution of the equation (9).

Once, the depth of flow at the base of weir model h_1 is obtained, it represents the initial depth of the hydraulic jump.

Darcy-Weisbach friction factor at the toe of the jump can be calculated using another iterative scheme.

The initial estimate of the friction factor, f_1, is made using the following form of the fully rough flow given by Keulegan [8]:

$$f_1 = \frac{1}{\left[2.03 \text{ Log } \left(\frac{K_s}{11.9\ h_1}\right)\right]^2} \qquad (11)$$

where, K_s is the Nikuradse sand roughness. If the grain size is uniform, then the roughness height is equal to the grain diameter. In natural beds of uniform materials the bed becomes armoured with larger particles, and by experience one can select the proper particle size, such as $K_s = \Delta$ or K_{65} whatever is appropriate. In the present study the value of K_s is taken to be the roughness height Δ ref. [1].

According to Colebrook-White [2] the formulas of the friction factor f_1 for the three types of fully developed turbulent flow are represented by the following :

1. Hydraulically smooth turbulent flow:

the friction factor is given by,

$$f_1 = \frac{1}{\left[2.0 \text{ Log } \left(\frac{R_{e1}\sqrt{f_1}}{2.51}\right)\right]^2} \qquad (12)$$

2. Transition region between hydraulically smooth and rough flows:

f_1 can be estimated by a modified Colebrook formula which is given by,

$$f_1 = \frac{1}{\left[2 \text{ Log}\left(\frac{\Delta}{12R_1} + \frac{2.5}{R_{e1}\sqrt{f_1}}\right)\right]^2} \qquad (13)$$

3. Hydraulically Fully Rough flow:

the friction factor can be estimated by,

$$f_1 = \frac{1}{\left[2.0 \text{ Log } \left(\frac{12\ R_1}{\Delta}\right)\right]^2} \qquad (14)$$

in which,

$R_{e1} = \frac{4\ U_1\ R_1}{\nu}$, Reynolds number for the open channel flow at the jump toe.

R_1 = hydraulic radius at the jump toe, and

Δ = The effective roughness height.

These three types of flow are distinguished from each other by the roughness Reynolds number which is based on the roughness height Δ and the shear velocity U_{*1}. This is given by

$$R_{*1} = \frac{U_{*1}\ \Delta}{\nu} \qquad (15)$$

where:

ν = kinematic viscosity.

The transition range of the roughness Reynolds number is approximately defined by the limits,

$$4. < \frac{U_{*1}\,\Delta}{\nu} < 100 \qquad (16)$$

The lower limit of the roughness Reynolds number marks the end of the smooth conditions while the upper limit indicates the beginning of fully rough conditions.

In order to measure the rate of convergence for the calculation of the friction factor in the iterative procedure, the difference between each two successive iterates, $(f_{1(n+1)} - f_{1(n)}) / f_{1(n)}$ is obtained. The smaller this difference becomes, the closer the iteration scheme gets to the proper solution. The convergence criterion is represented by the following [ref.7]:

$$\left| \frac{f_{1(n+1)} - f_{1(n)}}{f_{1(n)}} \right| \leq 0.000001 \qquad (17)$$

where :

$f_{1(n+1)}$ = the value of friction factor at the jump toe f_1 obtained after the number $n+1$ of the iteration cycles, and $f_{1(n)}$ is the respective value obtained after the number n of the iteration cycles.

This is considered to be a reliable indicator of the convergence of the iterative scheme.

Having obtained the local friction factor f_1 at the inlet section of the hydraulic jump, one also calculate the upstream Froude number F_1,

Since $$U_1 = q/h_1 \qquad (18)$$

then,

$$F_1 = \frac{U_1}{\sqrt{g h_1}} \qquad (19)$$

The values of friction factor f_1 and Froude number F_1 at the jump inlet section may now be adopted to find the properties of the hydraulic jump. According to the theoretical relations of ref. [1] for the rough bed hydraulic jump,

the relative jump length (L_j/h_1):

$$\frac{L_j}{h_1} = \frac{b - \sqrt{b^2 - 4\,a\,c}}{2\,a} \qquad (20)$$

where,

$$a = k_j \left\{ \left(\frac{f_1}{48}\right)^2 F_1^4 J^6 \left[2 + \frac{1}{J} \right]^2 - F_1^4 \frac{1}{k_j} (J+1)^6 \right\} \qquad (21)$$

$$b = k_j \left\{ \frac{f_1}{24} \left[J^3 (1 - J) + \frac{1}{2} F_1^2 J (J^2 - 1) \right] F_1^2 J^3 \left[2 + \frac{1}{J} \right] \right\} \qquad (22)$$

$$c = \left\{ kj \left[J^3(1-J) + \frac{1}{2} F_1^2 J(J^2-1) \right]^2 - F_1^4 (J+1)^3 (J-1)^2 \right\} \quad \text{.....(23)}$$

in which, kj is a dimensionless constant for the jump length which is equal to 35,000 ref. [6].

the conjugate depth ratio (J=h2/h1):

$$J = 2\sqrt{\frac{A}{3}} \cos\left[\frac{\Phi}{3}\right] \quad (24)$$

where,

$$\Phi = \cos^{-1}\left[\frac{-B}{2\sqrt{A^3/27}}\right] \quad (25)$$

$$J = h_2/h_1, \quad (26)$$

$$A = 1 + 2F_1^2 - \frac{f_1}{8} F_1^2 \left(\frac{Lj}{h_1}\right), \quad (27)$$

and $$B = 2F_1^2 \quad (28)$$

the relative integrated bed shear force (Pf/P1):

$$P_f/P_1 = (J-1)\left[\frac{2F_1^2}{J} - (1+J)\right] \quad (29)$$

where,

P_1= the hydrostatic pressure force at the jump toe which is given by ($0.5\,\gamma h_1^2$).

the total relative energy loss (EL/h1):

$$E_L/h_1 = \left\{1 - J + \frac{1}{2} F_1^2 \left[1 - \frac{1}{J^2}\right]\right\} \quad (30)$$

This will determine the various parameters of the hydraulic jump occurring over the different types of bed roughness. Therefore this theoretical model provides a computational approach for predicting the hydraulic jumps occurring over beds of various surface roughnesses. The larg. number of repetitive calculations involved in this numerical scheme indicates the necessity of a computer program to suit this theoretical model. The scheme adopted to solve the equations of the theoretical model in the computer program is given in Fig. 2.

3. Analysis and Discussion of the Results

The results of the various parameters of the hydraulic jump obtained using both the mathematical model and the experimental investigation ref [1] are plotted in the figures.

In order to check the reliability of the present theoretical model, the respective results are compared with the experimental data. The following analysis are made.

3.1 The Conjugate Depth Ratios, (h_2/h_1)

The ratio of the tailwater depth h_2 to the initial depth h_1 of the free hydraulic jump is called the conjugate depth ratio. The experimental data for the conjugate depth ratio are represented by the points in Figs. 3 to 8 for the different types of test beds. The curves in these figures represent the results of the theoretical model based on Eq. 24. The comparison shows fairly good agreement between both the measured and predicted values over the smooth test bed. In this case the predicted results are slightly better at high Froude number than those obtained from Bélanger Eqn. as shown in Fig. 3.

The figures also show that the depth ratios decreases when the test bed roughness height is increased.

For the rough test beds, the agreement between the theoretical model and the experimental results is fair in the range of Froude number of up to about 8. However, the predicted values of the conjugate depth tend to be higher than the measured values. Perhaps, this is because of the assumptions made to simplify the theoretical model as well as the error involved in the measurement of water depths of the hydraulic jump. The experimental difficulties such as the determination of the end of the jump due to the fluctuating nature of the tailwater may be the cause of such error in the depth ratio of the jump.

It is to be pointed out here that in all the experimental runs of the present study the jump begins to form at the foot of weir model, where the boundary layer is fully developed. Leutheusser and Kartha [4] have demonstrated that the effect of inflow condition (dependent on the boundary friction) changes the jump characteristics. This effect may be the cause of some of the deviations between the theoretical and the experimental results for the flows of high Froude number.

It is also noted from the figures that at low Froude numbers, the experimental points in the figures lie close to the line of Bélanger equation, which represents the smooth boundary conditions, then fall progressively further below the lines of the theoretical prediction as the Froude numbers increase. This trend is consistent with the findings of Leutheusser and Schiller [5] at very low Froude numbers, ($F_1<4$), where h_2/h_1 values for rough channels are often observed to be slightly above the line representing smooth boundary conditions.

Rajaratnam [9] interpreted these findings as being due to the separation of the boundary layer at the upstream section of the jump with a change in shear stress at the point of separation. Therefore, the net shear force might near zero or might be contributing to an increase in the subcritical sequent depth which, cause an increase in h_2/h_1 values.

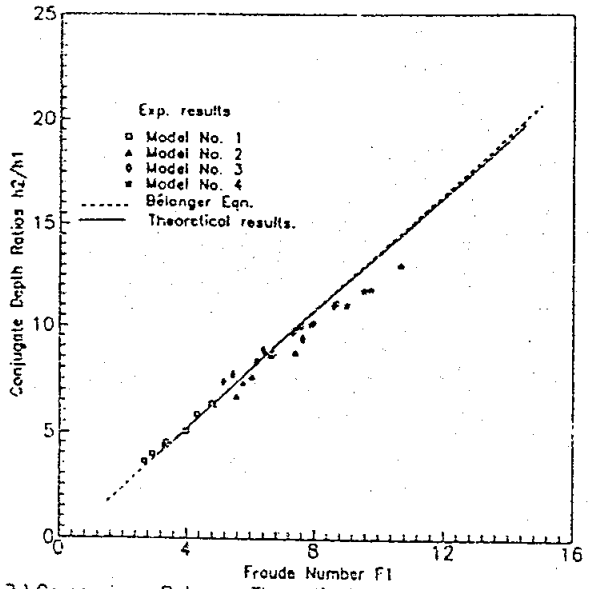

Fig. (3) Comparison Between Theoretical and Experimental Results for Conjugate Depth Ratio over Smooth Test Bed.

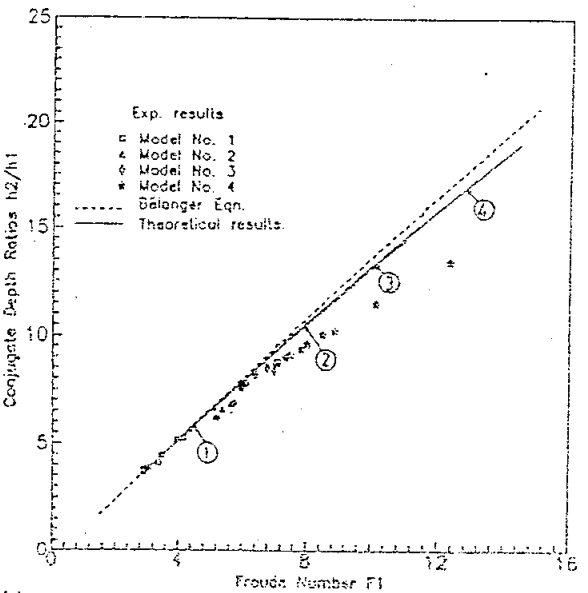

Fig. (4) Comparison Between Theoretical and Experimental Results for The Conjugate Depth Ratio over 1.0 −2.0 mm Test Bed.

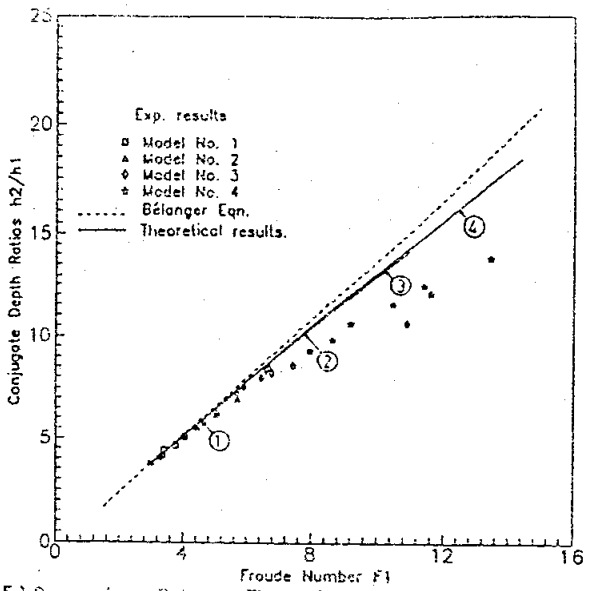

Fig. (5) Comparison Between Theoretical and Experimental Results for The Conjugate Depth Ratio over 2.0 –4.0 mm Test Bed.

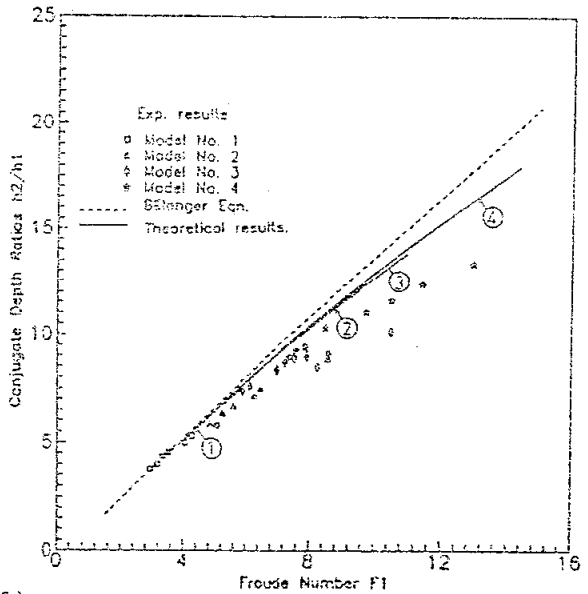

Fig. (6) Comparison Between Theoretical and Experimental Results for The Conjugate Depth Ratio over 4.00 – 4.75 mm Test Bed.

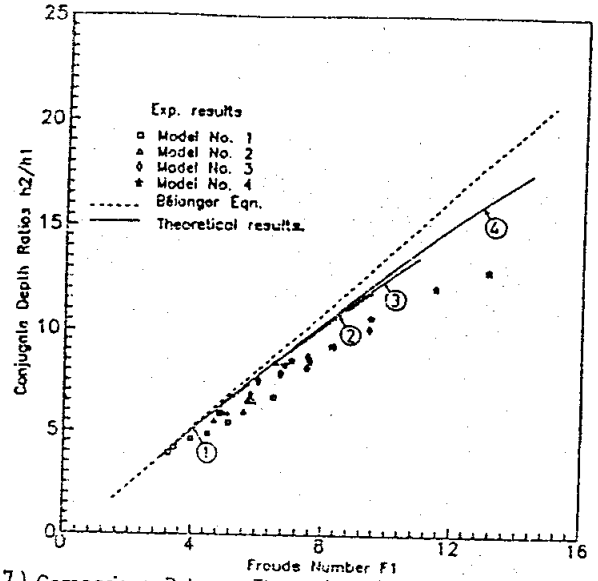

Fig. (7) Comparison Between Theoretical and Experimental Results for The Conjugate Depth Ratio over 4.75 – 9.5 mm Test Bed.

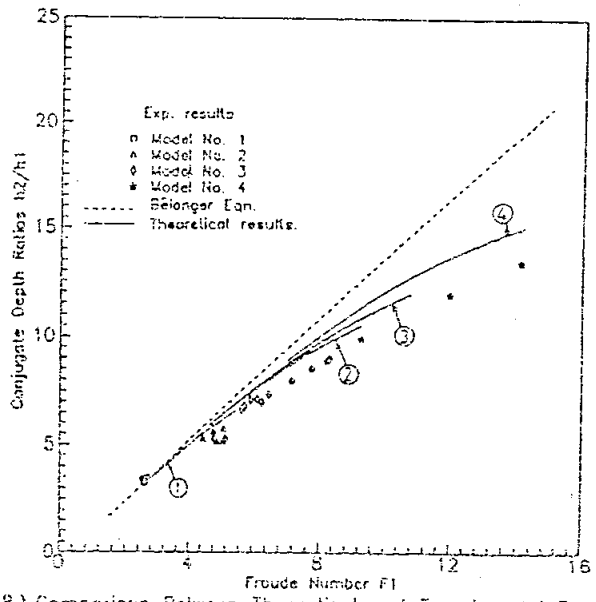

Fig. (8) Comparison Between Theoretical and Experimental Results for The Conjugate Depth Ratio over 12.5 – 19 mm Test Bed.

3.2 The Relative Jump Length, (L_j/h_1)

Figs. 9 to 14 show the comparison between the theoretical and experimental results for relative jump length L_j/h_1 over the different types of test beds. Fig. 9 shows good agreement between the measured values and the predicted results of the present theoretical model and the equation of Mehrotra. However, Mehrotra's results seems to be slightly closer to the experimental points of the smooth bed jump particularly for flows of high Froude number ($F_1 > 8$) as shown in Fig. 9.

The results of the present theoretical model for the relative jump length L_j/h_1 of the rough test beds display the effect of the bed roughness on the results when compared with Mehrotra's equation. However, some deviation exist between these predicted values and the experimental measurements. Perhaps this is due to the effect of both the assumptions made to simplify the theoretical model and the experimental error in the measurements of the relative length of the jump L_j/h_1. The figures also show a noticeable reduction in the jump relative length with the increased size of the test bed roughness. A falling trend of the relative jump length L_j/h_1 with the Froude number F_1 is observed for the test beds with rough element of large size (4.75-9.5 mm test bed and 12.5-19.0 mm test bed). This is expected because of the increasing value of the friction factor with the corresponding increase of the relative roughness at the jump toe Δ/h_1.

3.3 The Relative Energy Loss, (E_L/h_1)

Figs. 15 to 20 show a comparison between theoretical and experimental results for relative energy loss E_L/h_1 over the different types of test beds. Fig. 15 shows good agreement between the experimental results and the predicted values of the present theoretical model over the smooth bed.

For rough test beds Figs. 16 to 20 display fair agreement between the experimental and the theoretical predictions.

These figures also show that the results of the relative energy loss obtained from the present theoretical model are more accurate when compared with the respective results obtained from the equation of the classical jump.

3.4 The Relative Integrated Bed Shear Force, (P_1/P_1)

Figs. 21 to 26 show a comparison between the theoretical and the experimental results for the relative integrated shear force P_1/P_1. For the smooth test bed, Fig. 21 shows scattering of the experimental data about the predicted curves of the theoretical model. Perhaps, this is due to the sensitivity of the calculations of bed shear force over the smooth test bed using the one-dimensional momentum equation.

For the rough test beds, although Figs. 22 to 26 show agreement between the trend of both the experimental and the predicted results, the latter seems to be low when compared with experimental results. However, this deviation between the experimental results decreases with the increased size of roughness.

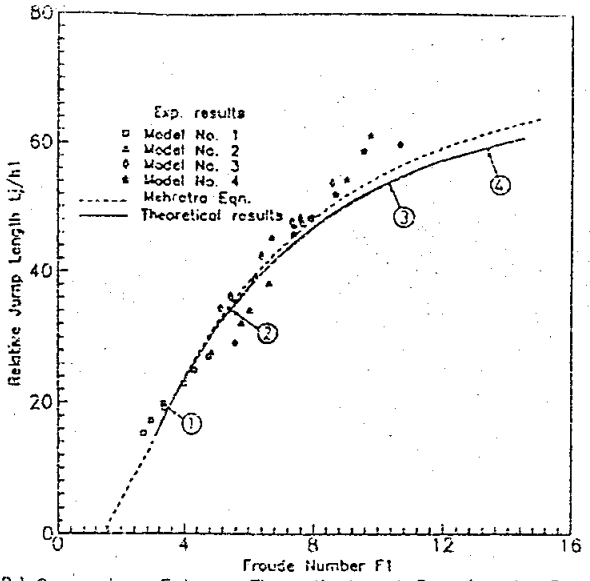

Fig. (9) Comparison Between Theoretical and Experimental Results for Relative Jump Length over Smooth Test Bed

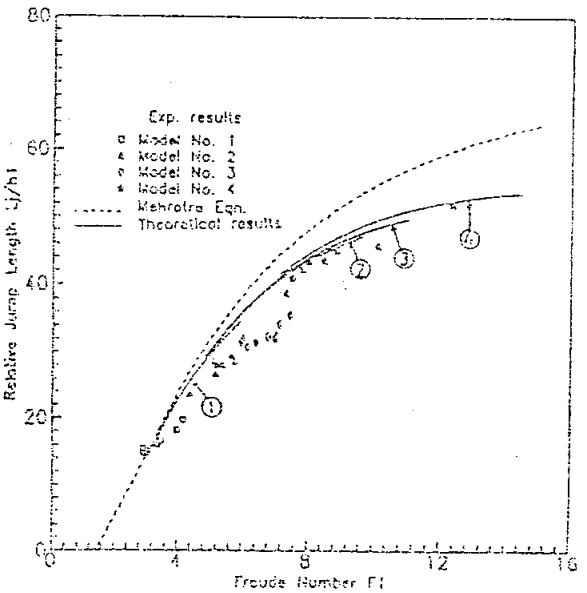

Fig. (10) Comparison Between Theoretical and Experimental Results for Relative Jump Length over 1.0-2.0 mm Test Bed

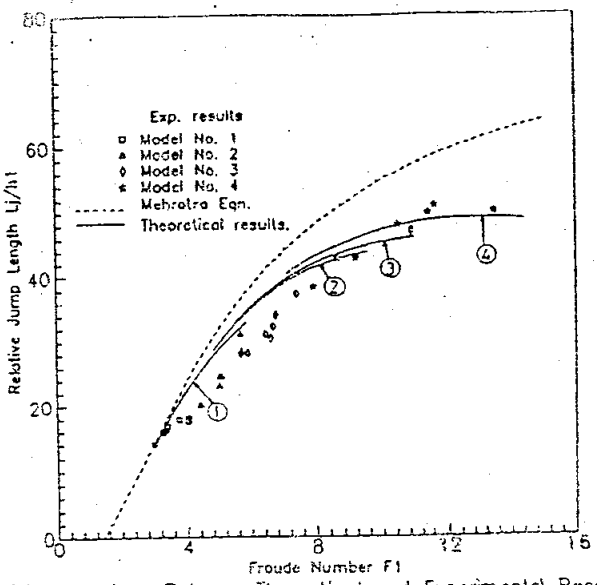

Fig. (11) Comparison Between Theoretical and Experimental Results for Relative Jump Length over 2.0–4.0 mm Test Bed

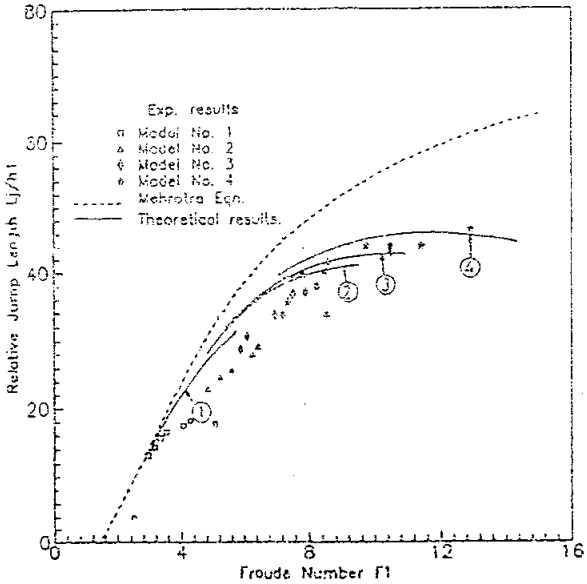

g. (12) Comparison Between Theoretical and Experimental Results for Relative Jump Length over 4.0–4.75 mm Test Bed

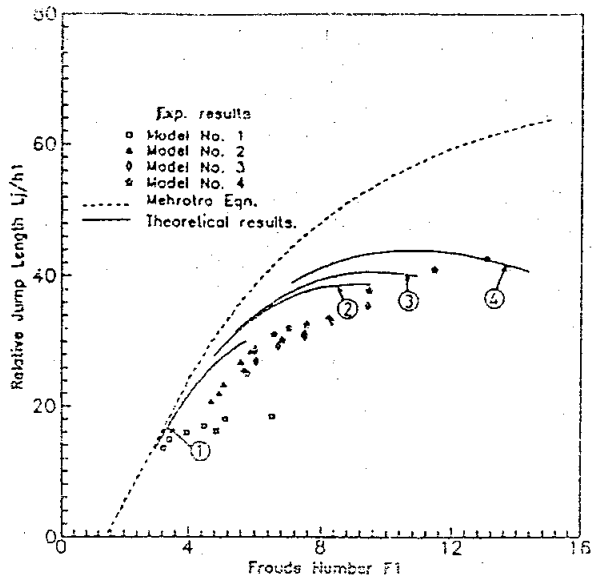

Fig. (13) Comparison Between Theoretical and Experimental Results for Relative Jump Length over 4.75–9.5 mm Test Bed

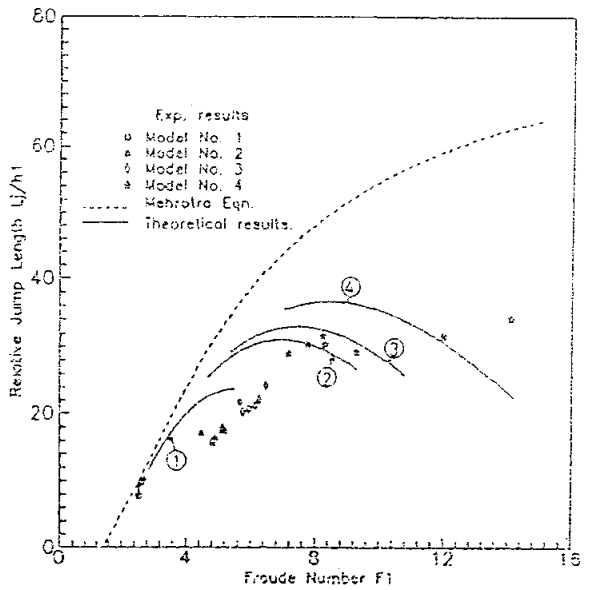

Fig. (14) Comparison Between Theoretical and Experimental Results for Relative Jump Length over 12.5–19.0 mm Test Bed

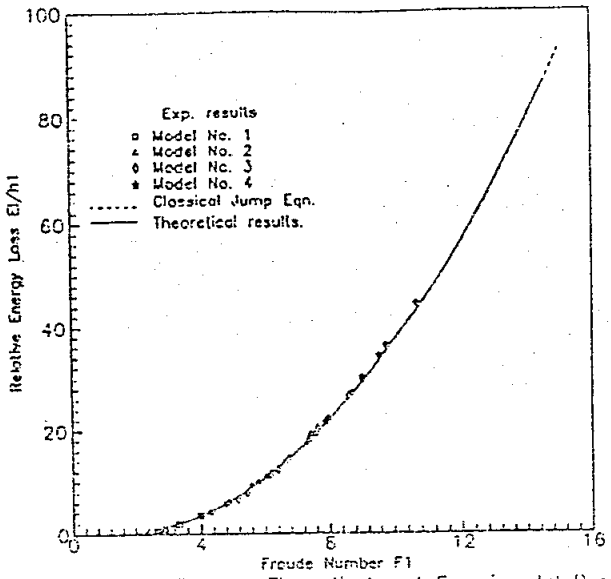

Fig. (15) Comparison Between Theoretical and Experimental Results for Relative Energy Loss over Smooth Test Bed

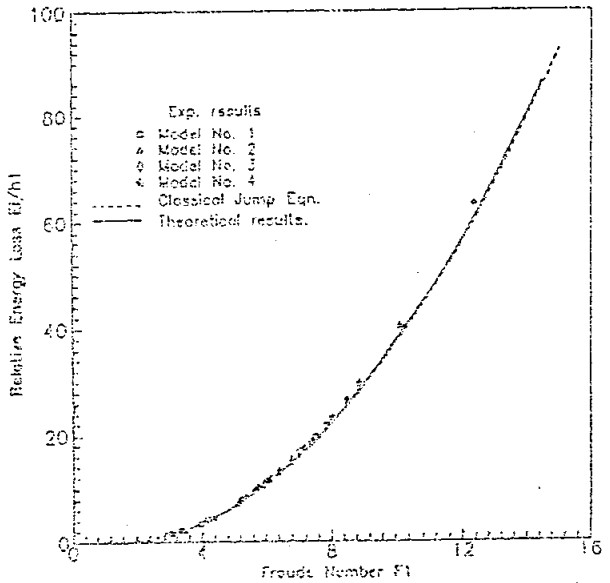

Fig. (16) Comparison Between Theoretical and Experimental Results for Relative Energy Loss over 1.0-2.0 mm Test Bed

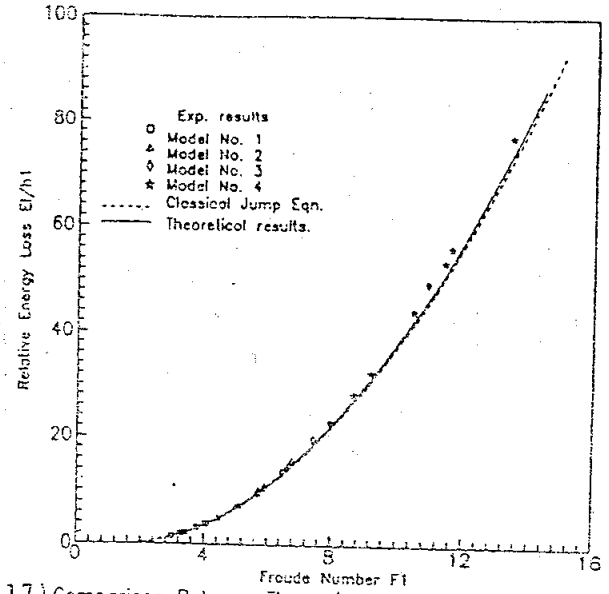

Fig. (17) Comparison Between Theoretical and Experimental Results for Relative Energy Loss over 2.0–4.0 mm Test Bed

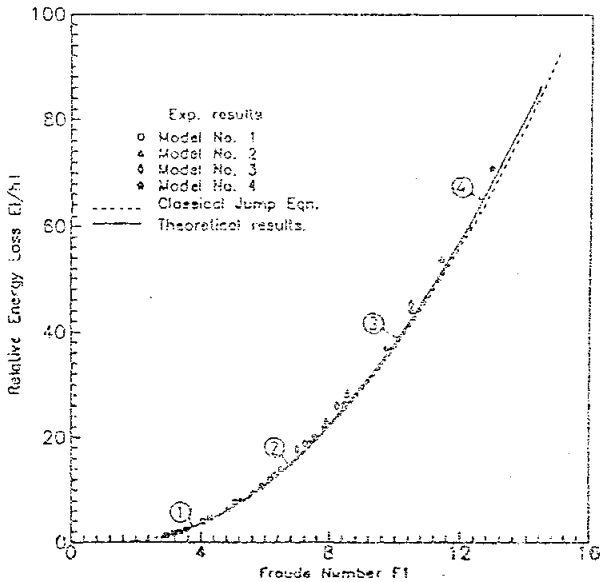

Fig. (18) Comparison Between Theoretical and Experimental Results for Relative Energy Loss over 4.0–4.75 mm Test Bed

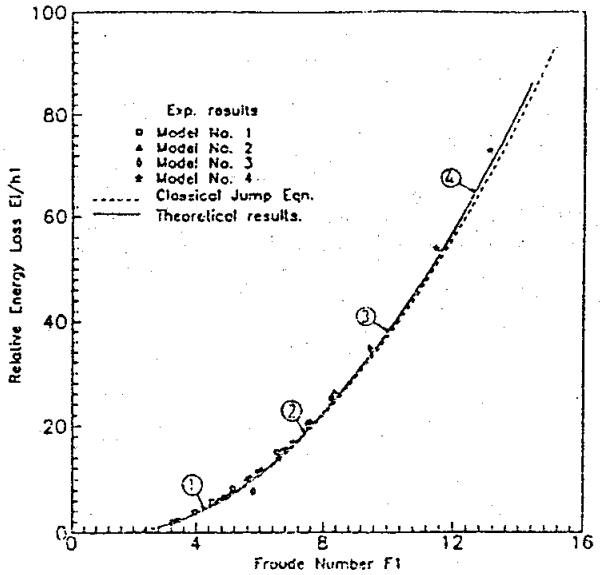

Fig. (19) Comparison Between Theoretical and Experimental Results for Relative Energy Loss over 4.75–9.5 mm Test Bed

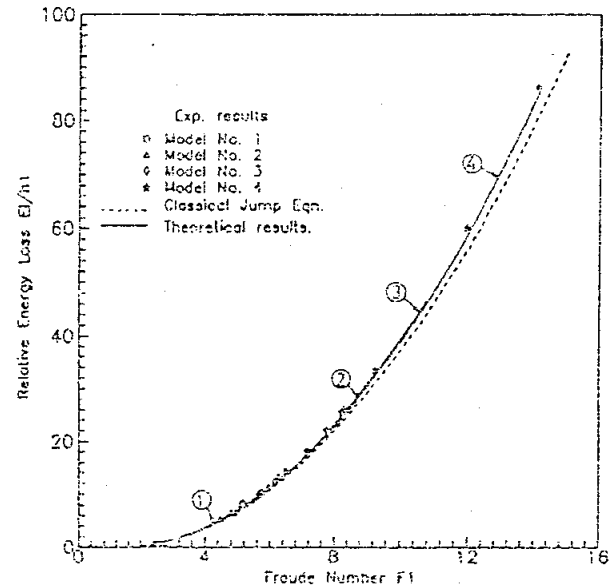

Fig. (20) Comparison Between Theoretical and Experimental Results for Relative Energy Loss over 12.5–19.0 mm Test Bed

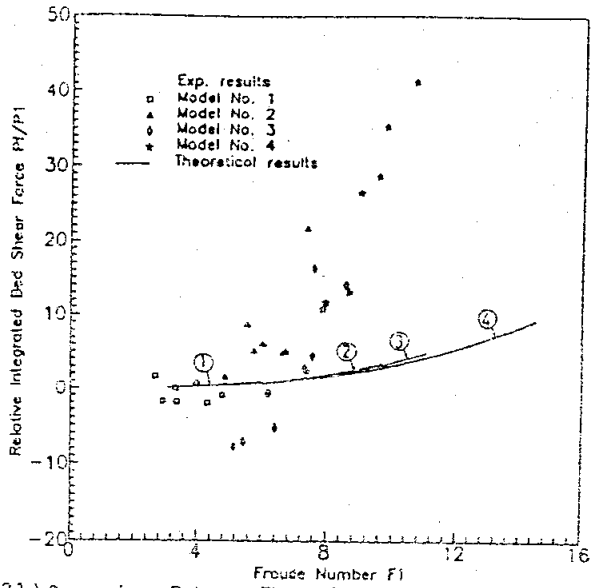

Fig. (21) Comparison Between Theoretical and Experimental Results for Relative Integrated Bed Shear Force over Smooth Test Bed

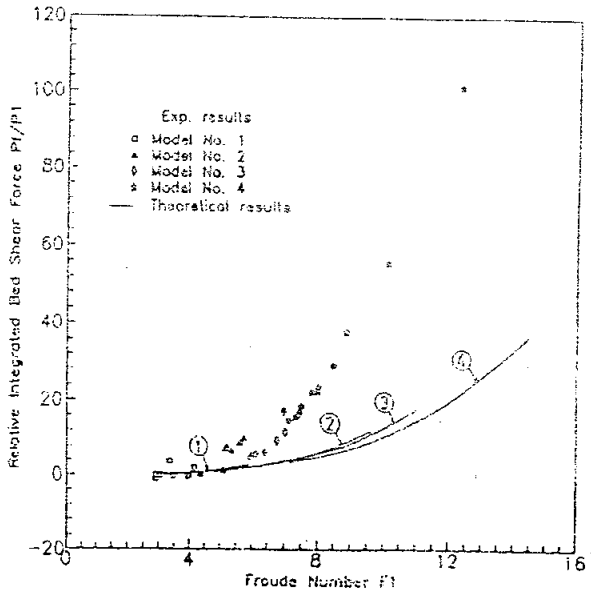

Fig. (22) Comparison Between Theoretical and Experimental Results for Relative Integrated Bed Shear Force over 1.0-2.0 mm Test Bed

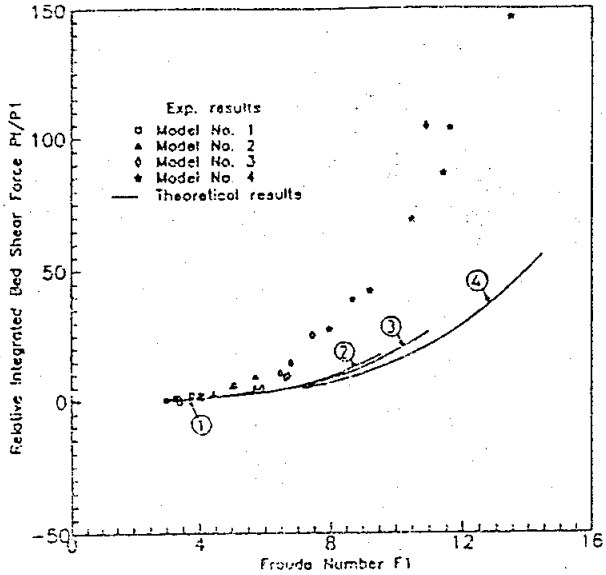

Fig. (23) Comparison Between Theoretical and Experimental Results for Relative Integrated Bed Shear Force over 2.0–4.0 mm Test Bed

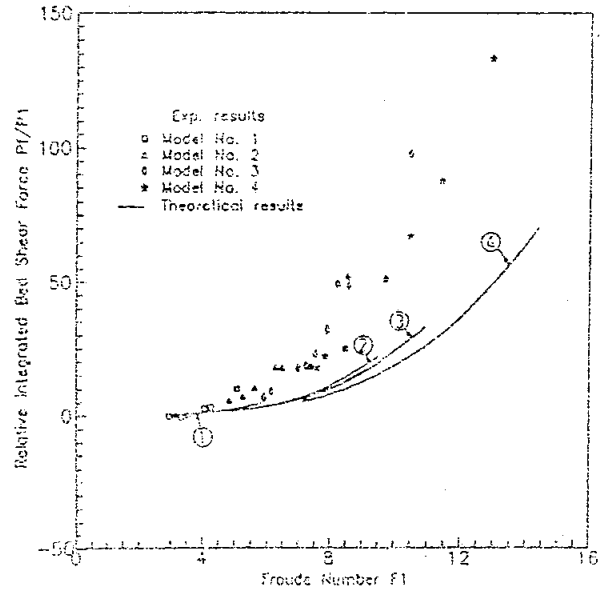

Fig. (24) Comparison Between Theoretical and Experimental Results for Relative Integrated Bed Shear Force over 4.0–4.75 mm Test Bed

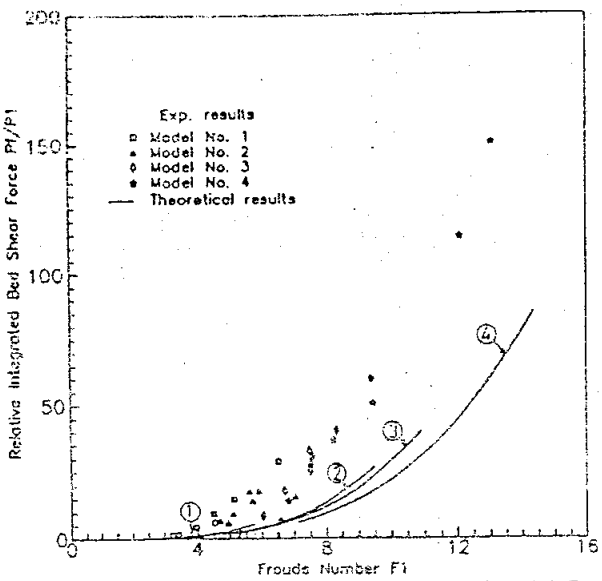

Fig. (25) Comparison Between Theoretical and Experimental Results for Relative Integrated Bed Shear Force over 4.75–9.5 mm Test Bed

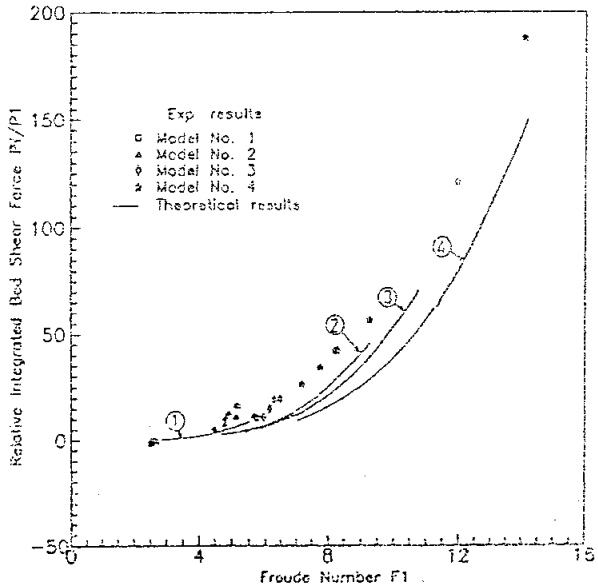

Fig. (26) Comparison Between Theoretical and Experimental Results for Relative Integrated Bed Shear Force over 12.5–19.0 mm Test Bed

The Figs. 21 to 26 also show increasing value for the relative integrated bed shear force with the increasing of the size of bed roughness.

4. CONCLUSIONS

The following are the conclusions made from the comparesion of both the theoretical and experimental studies.

The trend of the experimental results is consistent with the theoretical prediction, and some good agreement between the results is achieved in the present study. The theoretical results also show some deviations from the experimental results for some of the parameters of the hydraulic jump particularly for the flows of high Froude number over the rough bed. However, the theoretical prediction may be improved by the actual representation of the friction distribution on the rough test bed in the theoretical relations representing the rough beds. The effect of the fully developed inflow conditions at the jump toe must be also considered in the theoretical analysis of the jump.

REFERENCES

1. El-Feki, A. M., "Effect of the Bed Sand Roughness on the Geometry of the Hydraulic Jump", M. Sc. Thesis, University of El-Mansoura, March, 1990.

2. French, R. H., "Open-Channel Hydraulics", McGraw-Hill Book Co., Singafore, 1986.

3. Lawson, J. D., and Phillips, B. C., "Circular Hydraulic Jump", Journal of Hydraulic Engineering, Vol. 109, No. 4, April, 1983, paper No. 17889, pp. 505-518.

4. Leutheusser, H. J. and Kartha, V.C., "Effects of Inflow Condition on Hydraulic Jump", Journal of the Hydraulics Division, ASCE, Vol. 98, No. HY8, proc. paper 9088, Aug. 1972, pp. 1367-1385.

5. Leutheusser, H. J. and Schiller, E.J., "Hydraulic Jump in a Rough Channel", Water Power and Dam Construction, Vol. 27, No. 5, May, 1975, pp. 186-191.

6. Mehrotra, S. C., "Length of Hydraulic Jump", Journal of the Hydraulics Division, ASCE, Vol. 102, No. HY7, proc. paper 12272, July 1976, pp. 1027-1033.

7. Mironer, Alan, "Engineering Fluid Mechanics", McGraw-Hill International Book Company, Kogakusha, Ltd., for manufacture and export, 1979, pp. 475-482.

8. Raudkivi, A. J., "Loose Boundary Hydraulics", Robert Maxwell publisher, London, 1976.

9. Rajaratnam, N., "The Hydraulic Jump as a Wall Jet", Journal of the Hydraulics Division, ASCE, Vol. 91, No. HY5, proc. paper 4482, September, 1965, pp. 787-795.

10. Tung, Yeou-Koung, and Mays, Larry, W., "Optimal Design of Stilling Basins for over Flow Spillways", Journal of the Hydraulics Division, ASCE, Vol. 108, No. HY10, Oct. 1982, pp. 1163-1178, paper 17398.

APPENDIX I : NOTATIONS.

The following symbols are used in this paper,

Symbol	Definition
A	Parameter given by Eq. 27.
a	Parameter given by Eq. 21.
B	Parameter given by Eq. 28.
b	Parameter given by Eq. 22.
c	Parameter given by Eq. 23.
C_o	Discharge coefficient.
C_v	Coefficient of velocity.
E_o	Specific energy at section 0-0.
E_1	Specific energy at section 1-1.
E_L	Total energy loss over any test bed.
f_1	Darcy-Weisbach friction factor at jump toe.
F_1	Supercritical Froude number, $U_1/\sqrt{gh_1}$.
H	Head over weir model, Fig. 1.
h_1	Effective depth of flow at the jump toe.
h_2	Effective depth of flow at the jump heel.
$h_{L_{o-1}}$	The energy loss across the weir model .
J	Conjugate depth ratios, h_2/h_1.
k_j	Constant for jump length, Eqs.21, 22, 23
k_s	Equivalent sand grain roughness (Nikuradse).
L_j	Length of jump, Fig. 1.
P	Height of weir model.
P_1	Pressure force per unit width at jump toe.
P_f	Integrated bed shear force per unit width
Q	Discharge, V/T.
R_1	Hydraulic radius at jump toe.
R_{e1}	Reynold's number at jump toe, $4U_1R_1/\nu$.
R_{*1}	Reynold's number for roughness, $U_{*1}\Delta/\nu$.
U_{*1}	Shear velocity at jump toe, $\sqrt{\tau_{o1}/\rho}$.
W	Width of channel.
Z	Drop height of weir model.
Z_o	Effective drop height of weir model, (Z-Δ).
γ	Specific weight of water.
Δ	Effective height of roughness elements,
μ	Dynamic viscosity.
ν	Kinematic viscosity.
ρ	Density.
τ	Parameter given by Eq. 25

APPENDIX II: THE MODEL COMPUTER PROGRAM LISTING.

```
C*******COMPUTER MODEL FOR HYDRAULIC JUMP OVER ROUGH BEDS.**********
      REAL JO,KJ,KR,J,LJH1,LRH1,LRH2,LJH2,LJ,LR,NU
      REAL K(10),MO(10),DELTA(10),CO(10),CV(5)
      DIMENSION Z(10),Q(40),DMAX(10),DMIN(10),H(40),DMEAN(10)
C     INPUT DATA
      KJ=35000.
      KR=20000.
      NU=1.07E-6
      BF=0.61
      G=9.81
      CV(1)=0.79
      CV(2)=0.85
      CV(3)=0.75
      CV(4)=0.8
      PI=3.141592653589793
C     ************* DATA FOR WEIR MODEL NO.1 **********************
      Z(1)=.11
      CO(1)=2.363345
      MO(1)=1.657772
C     ************* DATA FOR WEIR MODEL NO.2 **********************
      Z(2)=.223
      CO(2)=2.1481524
      MO(2)=1.696227
C     ************* DATA FOR WEIR MODEL NO.3 **********************
      Z(3)=.325
      CO(3)=1.8172884
      MO(3)=1.665276
C     ************* DATA FOR WEIR MODEL NO.4 **********************
      Z(4)=.43
      CO(4)=1.1835774
      MO(4)=1.522367
C     RANGE OF DISCHARGES
      Q(1)=0.004
      DO 66 I=2,9
      Q(I)=Q(I-1)+0.002
   66 CONTINUE
C     PROPERTIES OF BED MATERIALS
      DMAX(1)=1.E-5
      DMAX(2)=0.002
      DMAX(3)=0.004
      DMAX(4)=0.00475
      DMAX(5)=0.0095
      DMAX(6)=0.019
      DMIN(1)=1.E-5
      DMIN(2)=0.001
      DMIN(3)=0.002
      DMIN(4)=0.004
      DMIN(5)=0.00475
      DMIN(6)=0.0125
C     CALCULATION OF D FOR THE DIFFERENT TEST BEDS
      DO 88 I=1,6
      DMEAN(I)=(DMAX(I)+DMIN(I))/2.
```

```
          IF(DMEAN(I).LE.0.0045) K(I)=DMEAN(I)
          IF(DMEAN(I).GT.0.0045) K(I)=0.8*DMEAN(I)
     88   CONTINUE
          DO 3 I=1,4
C         WRITE OF HEADINGS ***********************************************
          WRITE(6,111) Z(I)
    111   FORMAT(//,30X,'DROP HEIGHT  Z=',F10.5)
          DO 4 M=1,6
          WRITE(6,222)DMAX(M),DMIN(M),DMEAN(M),K(M)
    222   FORMAT(//,3X,'DMAX=',F7.5,4X,'DMIN=',
         #  F7.5,4X,'DMEAN=',F7.5,4X,'ROUGHNESS HEIGHT=',F7.5/)
          WRITE(6,112)
    112   FORMAT(/5X,'F1',3X,'h2/h1',2X,'Lj/h1',
         &  3X,'EL/h1',3X,'Pf/P1')
          DO 5 L=1,8
          QS=Q(L)/BF
          H(L)=(Q(L)/CO(I))**(1./MO(I))
C         CALCULATION OF THE EFFECTIVE DROP HEIGHT (ZACT) **************
          ZACT=Z(I)-.0015-K(M)
C         CALCUTATION OF THE INITIAL DEPTH OF THE JUMP (H1)
          H1=.9*HC
          MM=1
    555   H1NEW=Q(L)/(CV(I)*BF*SQRT(2.*G*(H(L)+ZACT-H1)))
          TEST1=ABS(H1NEW-H1)
          IF(TEST1-0.0000000001) 1,1,55
     55   IF(MM.GT.50) GO TO 1
          MM=MM+1
          H1=H1NEW
          GO TO 555
C         CALCULATION OF THE SUPERCRITICAL FROUDE NUMBER (F1)
      1   F1=QS/SQRT(G*H1**3)
          V1=QS/H1
          AREA=H1*BF
          PREM=BF+2.*H1
          HR=AREA/PREM
          R=K(M)/HR
C         CALCULATION OF THE FIRST ESTIMATE OF THE COEFFICIENT OF
C         FRICTION USING KUTTEGAN FORMULA
          FB=1./(2.03*ALOG10(K(M)/(R1*11.09)))**2
C         CALCULATION OF THE CORRECT VALUE OF THE COEFFICIENT OF
C         FRICTION.
          NN=1
          RE1=4.*HR*V1/NU
    999   VS1=SQRT(FB/8.)*V1
          RS1=VS1*K(M)/NU
          IF(RS1.LT.4.) FNEW=1./(2.*ALOG(RE1*SQRT(FB)/2.51))**2
          IF(RS1.GE.4.0.AND.RS1.LE.100.) FNEW=
         $ 1./(2.*ALOG((R/12.)+2.5/(RE1*SQRT(FB))))**2
          IF(RS1.GT.100.) FNEW=1./(2.*ALOG(12./R))**2
          TEST=ABS((FB-FNEW)/FB)
          IF(TEST-0.000001) 9,9,99
     99   IF(NN.GE.50) GO TO 9
          FB=FNEW
          NN=NN+1
          GO TO 999
```

```
    9   F=FB
C       CALCULATION OF THE INITIAL ESTIMATE OF THE VALUE OF (J)
        JO=.5*(SQRT(1.+8.*F1**2)-1.)
        N=1
C       ITERATIVE PROCEDURE TO IMPROVE THE VALUE OF (J)
   30   FUN=(F/48.)*F1**2*(2.+(1./JO))
        AJ=KJ*FUN**2*JO**6
        AA=(F1**4)*(JO+1.)**6
        BJ=2.*JO**3*FUN*(JO**3*(1.-JO)+.5*(F1**2)*JO*(JO**2-1.))*FUN
        CJ=KJ*(JO**3*(1.-JO)+.5*F1**2*JO*(JO**2-1.))**2
        D=F1**4*(JO+1.)**6*(JO-1.)**2
        IF((AJ-AA).EQ.0.0) GO TO 3
        ZZ=BJ**2-4.*(AJ-AA)*(CJ-D)
        SQR=SQRT(ZZ)
        LJH1=(BJ-SQR)/(2.*(AJ-AA))
        A=1.+2.*F1**2-(F/8.)*LJH1*F1**2
        B=2.*F1**2
        AMR=(-B/(2.*SQRT(A**3/27.)))
        IF(AMR.GT.1.0.OR.AMR.LT.-1.0) GO TO 3
        PHI=ACOS(AMR)
        J=2.*SQRT(A/3.)*COS(PHI/3.)
        DIFF=ABS(JO-J)
        IF(DIFF.LT.0.0000000001) GO TO 100
        IF(N.GT.50) GO TO 100
        JO=J
        N=N+1
        GO TO 30
  100   AR=AJ*(KN/KJ)
        BR=BJ*(KN/KJ)
        CR=CJ*(KN/KJ)
        LRH1=(BR-SQRT(BR**2-4.*(AR-AA)*(CR-D)))/(2.*(AR-AA))
        LJH2=LJH1/J
        LRH2=LRH1/J
        PFP1=(J-1.)*(2.*F1**2/J-(1.+J))
        ELH1=1.0-(0.5*(F1/J)**2*(J**2-1.0)
        EEN1=(F)**2/SQRT(FJ))*(((J+1.0)/J)**3)
     #  *SQRT(LJH1**2+(J-1.0)**2)
        EFH1=FUN*LJH1
C       PRINT PROGRAM RESULTS
        WRITE(6,20)F1,J,LJH1,ELH1,PFP1
   20   FORMAT(1X,5(1X,F7.3))
    5   CONTINUE
    4   CONTINUE
    3   CONTINUE
        STOP
        END
```